J Appl Electrochem (2014) 44:1165–1170
DOI 10.1007/s10800-014-0743-6

SHORT COMMUNICATION

Ni nanoparticles-graphene hybrid film: one-step electrodeposition preparation and application as highly efficient oxygen evolution reaction electrocatalyst

Zonghua Pu · Qian Liu · Abdullah M. Asiri · Xuping Sun

Received: 18 June 2014 / Accepted: 3 September 2014 / Published online: 9 September 2014

Abstract In this communication, we demonstrate the preparation of Ni nanoparticles-graphene hybrid film via simultaneous electrochemical reduction of graphene oxide and Ni^{2+} on conductive substrate for the first time. We further show the utilization of such hybrid film as an efficient oxygen evolution reaction electrocatalyst with highly catalytic activity and good durability.

Keywords One-step electrodeposition · Graphene film · Ni nanoparticles · Oxygen evolution reaction electrocatalysts

1 Introduction

Hydrogen is the most promising option to replace fossil fuels in the long-term owing to its carbon-free, high-energy content, and potential to be efficiently converted into either electrical or thermal energy. Electrolysis of water is currently an emerging technology to produce bulk hydrogen, and the kinetic bottleneck of water splitting is the oxygen evolution reaction (OER) [1, 2]. Thus, an efficient electrocatalyst is required to improve the reaction rate and lower the overpotential [3]. Many researchers are currently working on water oxidation catalysts [4]. Precious metal oxides such as RuO_2 and IrO_2 are the most active catalysts with the lowest overpotentials for the reaction at practical current densities, but their high cost and poor long-term stability in alkaline solution limit their widespread commercial use [5, 6]. As such, great efforts have been made to develop earth-abundant metal-based alternatives [7–11].

Ni is a promising candidate for replacing precious catalysts due to its high theoretical activity and low cost [12, 13], but it suffers from low efficiency and poor stability [14]. The use of conductive graphene sheets as supports can enhance electron transport and hence catalytic performance, and the direct deposition of electrocatalyst film onto electrode surfaces eliminates the immobilization step of catalyst. In this communication, we develop a one-step electrodeposition strategy toward rapid preparation of Ni nanoparticles-graphene hybrid film (NiNPs-G) on conductive substrate via simultaneous electrochemical reduction of graphene oxide (GO) and Ni^{2+}. We further demonstrate the use of such hybrid film as OER electrocatalyst with high efficiency and good durability.

2 Experimental

Graphite and H_2SO_4 were purchased from Aladdin Ltd. (Shanghai, China). $KMnO_4$ was purchased from Beijing Chemical Corporation. $NiSO_4{\cdot}6H_2O$ was purchased from Tianjin Fuchen Chemical Reagent Factory. Sodium citrate ($C_6H_5Na_3O_7{\cdot}2H_2O$) was purchased from Xilong Chemical Co. Ltd. All the chemicals were used as received without further purification. The water used throughout all experiments was purified through a Millipore system.

Z. Pu · Q. Liu · X. Sun
Chemical Synthesis and Pollution Control Key Laboratory of Sichuan Province, College of Chemistry and Chemical engineering, China West Normal University, Nanchong 637002, Sichuan, China

A. M. Asiri · X. Sun
Chemistry Department, Faculty of Science, King Abdulaziz University, Jeddah 21589, Saudi Arabia

A. M. Asiri · X. Sun (✉)
Center of Excellence for Advanced Materials Research, King Abdulaziz University, Jeddah 21589, Saudi Arabia
e-mail: sunxpcwnu@gmail.com

GO was prepared from natural graphite powder by Hummers method [15]. In a typical synthesis, 1 g of graphite was added into 23 mL of 98 % H_2SO_4, followed by stirring at room temperature (25 ± 2 °C) over a 24 h period. After that 100 mg of $NaNO_3$ was introduced into the mixture and stirred for 30 min. Subsequently, the mixture was kept below 5 °C in an ice bath, and 3 g of $KMnO_4$ was slowly added into the mixture. Then the mixture was stirred for another 30 min at 35–40 °C. After that 46 mL of water was added into the above mixture over a period of 25 min. Finally, 140 mL of water and 10 mL of 30 % H_2O_2 were added into the mixture to stop the reaction. After the unreacted graphite in the resulting mixture was removed by centrifugation, as-synthesized GO was dispersed into individual sheets in anhydrous ethanol at a concentration of 0.5 mg mL^{-1} with the aid of ultrasound for further use.

NiNPs-G was electrodeposited in solution of 2 mmol $NiSO_4{\cdot}6H_2O$, 3.5 mmol $C_6H_5Na_3O_7{\cdot}2H_2O$, and 1 mg mL^{-1} GO (pH value was controlled to 6.0 by adding Na_2CO_3) with current density of 0.5 mA cm^{-2} at 50 °C for 25 min. Fluorine-doped tin oxide (FTO) was used as working electrode for electrodeposition. A graphite electrode and an Ag/AgCl electrode were used as the counter electrode and reference electrode, respectively. The Ni nanoparticles (NiNPs) were also prepared by the same route without adding GO into deposition solution. The NiNPs or NiNPs-G loading on FTO was determined by reading the difference between bare FTO and NiNPs or NiNPs-G on FTO using a high-precision analytical balance. The mass loading of NiNPs and NiNPs-G was about 0.2 mg cm^{-2}.

Powder X-ray diffraction (XRD) data were recorded on a RigakuD/MAX 2550 diffractometer with Cu Kα radiation ($\lambda = 1.5418$ Å). Raman spectra were obtained on J-Y T64000 Raman spectrometer with 514.5 nm wavelength incident laser light. X-ray photoelectron spectroscopy (XPS) was carried out on an ESCALABMK II X-ray photoelectron spectrometer using Mg as the exciting source. Scanning electron microscopy (SEM) measurements were made on a XL30 ESEM FEG scanning electron microscope at an accelerating applied potential of 20 kV. Transmission electron microscopy (TEM) measurements were made on a Hitachi H-8100 electron microscope (Hitachi, Tokyo, Japan) with an accelerating voltage of 200 kV.

The electrochemical properties of the prepared electrocatalysts were studied in a standard three-electrode system with 0.1 M KOH aqueous solution. The NiNPs-G- or NiNPs-coated FTO was used as working electrode. An Ag/AgCl was used as reference electrode and a Pt wire as counter electrode. Electrochemical measurements were carried out on a CHI 660D electrochemical workstation. All electrochemical measurements were carried out at room temperature.

3 Results and discussion

Figure 1a shows the powder XRD pattern of the resulting electrodeposited products on FTO substrate. The diffraction peaks at 34 and 38° can be assigned to the (101) and (200) planes of FTO substrate (JCPDS no. 41-1445). The diffraction peaks at 45° can be assigned to metallic Ni. Figure 1b shows the Raman spectra of GO and the NiNPs-G obtained by electrodeposition. It is seen that both GO and the produced graphene exhibit two characteristic main peaks: the D band at ~1,356 cm^{-1}, arising from a breathing mode of A_{1g} symmetry involving phonons near the K zone boundary; the G band at ~1,595 cm^{-1}, origining from in-plane vibration of sp^2 carbon atoms and a doubly degenerate phonon mode (E_{2g} symmetry) at the Brillouin zone center [16].The G band of graphene redshifts from 1,602 to 1,595 cm^{-1}, which is attributed to the high ability for recovery of the hexagonal network of carbon atom [17]. It is also found that the graphene shows the relative higher intensity of D to G band (0.97) than that of GO (0.81). This change in the intensity ratio of the D to G bands is attributed to the increased defect concentration present in graphene relative to that in GO [18]. The deposition of graphene from GO suspension can be explained as follows [19]: GO in direct contact with FTO accepts electrons and is electrochemically reduced into graphene during cathodic scan. The poor solubility in water of these graphene sheets causes their direct attachment to FTO surface. Figure 1c shows the XPS C 1 s spectrum of the NiNPs-G, which indicates the presence of C–C (284.5 eV) and C–O (286.0 eV) [20]. The XPS Ni 2p spectrum (Fig. 1d) indicates that the binding energies of Ni $2p_{3/2}$ and Ni $2p_{1/2}$ peaks are located at 852.7 and 870.1 eV, respectively.

Figure 2a shows the low magnification SEM image of the NiNPs-G, indicating that a large amount of nanoparticles and graphene nanosheets are generated on the surface of conductive substrate. The high magnification SEM image reveals that the nanoparticles have sizes ranging from 30 to 90 nm, as shown in Fig. 2b. A high-resolution TEM (HRTEM) image of one single particle (inset) reveals a lattice fringe of 0.2 nm corresponding to the (111) plane of Ni, suggesting these nanoparticles are NiNPs. Pure NiNPs film was electrodeposited using the same procedure without adding GO, as shown in Fig. 2c. The high magnification SEM image shown in Fig. 2d further reveals that the NiNPs have sizes ranging from 50 to 100 nm. All these observations indicate the formation of NiNPs-G through the one-step electrodeposition process.

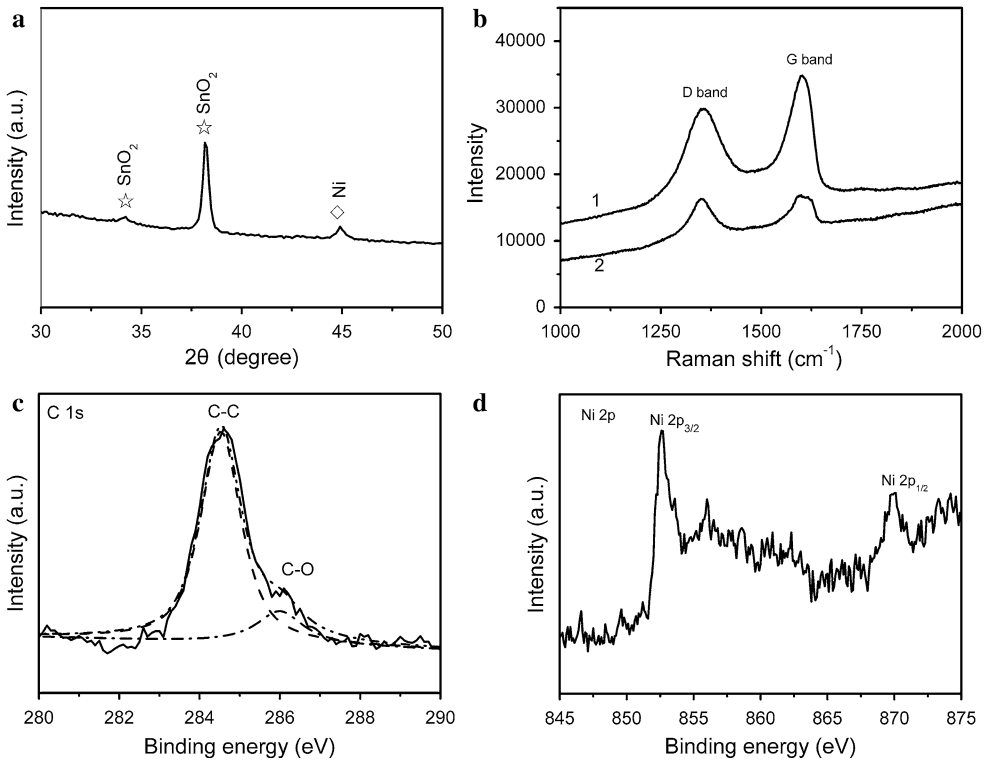

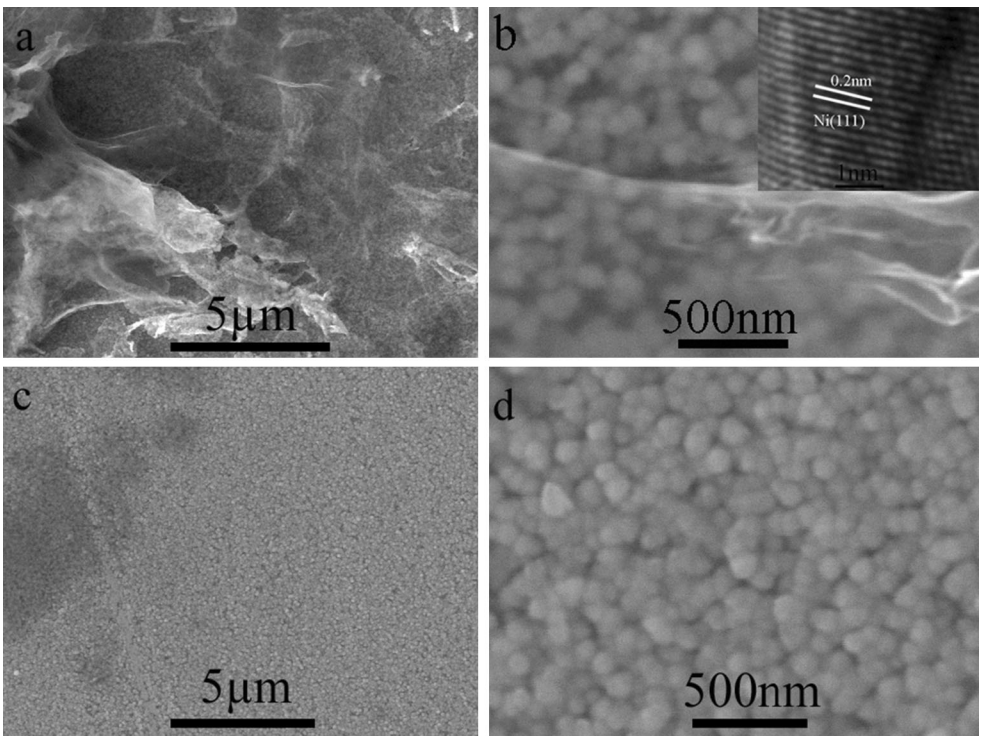

Fig. 1 **a** XRD pattern of FTO supported NiNPs-G. **b** Raman spectra of (*curve 1*) GO and (*curve 2*) the NiNPs-G. XPS analysis of (**c**) C 1 s spectrum and **d** Ni 2p spectrum for NiNPs-G

Fig. 2 **a** Low and **b** high magnification SEM images of NiNPs-G (*inset* HRTEM images taken from one single particle). **c** Low and **d** high magnification SEM images of NiNPs

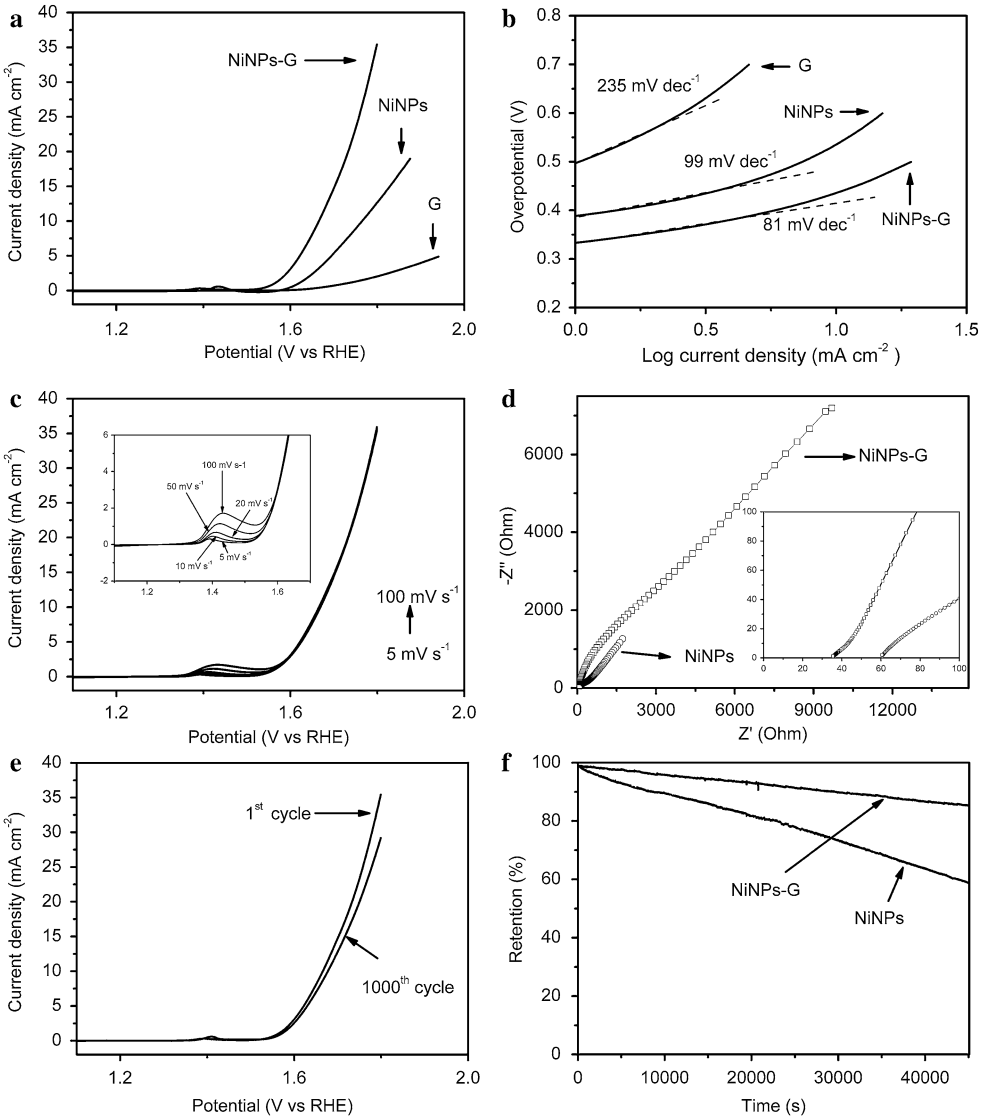

Fig. 3 **a** Polarization curves of NiNPs-G, NiNPs and graphene in 0.1 M KOH solution at a sweep rate of 5 mV s^{-1}. **b** Tafel plots of NiNPs-G, NiNPs and graphene. **c** Polarization curves of NiNPs-G at different scan rates. **d** Nyquist plots of the NiNPs-G and NiNPs. **e** OER polarization curves of NiNPs-G before and after CV test of 1,000 cycles. **f** Retention percentage of the catalytic current for NiNPs-G and NiNPs (1.614 V vs. RHE) during 45,000 s

The linear scan voltammograms (LSVs) measurements were used to test OER properties of NiNPs-G, NiNPs and graphene with a scan rate of 5 mV s^{-1} in 0.1 M KOH from 0.964 to 1.964 V versus RHE. Figure 3a shows polarization curves of these catalysts. For NiNPs-G, an extremely weak anodic wave near 1.394 V is observed, which is more negative than that of NiNPs (1.434 V). Graphene displays no apparent anodic waves. Note that NiNPs-G shows a more negative onset potential (1.564 V) than those of NiNPs (1.604 V) and graphene (1.634 V). The overpotential of NiNPs-G is 334 mV, which is only slightly higher than that of recent N-doped graphene film-confined NiNP (320 mV) [14]. The highly catalytic activity is demonstrated by comparing the current density of NiNPs-G with those of NiNPs and graphene. For achieving a catalytic current density of 5 mA cm^{-2}, the applied potentials need to be 1.622 V ($\eta = 392$ mV) and 1.694 V ($\eta = 464$ mV) for NiNPs-G and NiNPs, respectively. When the overpotential is 550 mV, NiNPs-G shows the largest catalytic current density (30.29 vs. 11.15 mA cm^{-2} for NiNPs and 1.72 mA cm^{-2} for graphene). These values compare favorably to the behavior of other non-noble OER electrocatalysts, including N-doped graphene-$NiCo_2O_4$ hybrid [21] and 3D Ni foam/porous carbon/anodized Ni [22]. All these results indicate that NiNPs-G is a highly active catalyst toward water oxidation. What's more, Tafel plots of the samples were recorded with the linear regions fitted into the Tafel equation ($\eta = a + b \log j$, where η is overpotential, b is the Tafel slope and j is the current density) [23]. As shown in Fig. 3b, the NiNPs-G shows the smallest Tafel slope value (81 mV dec^{-1}) among all the presented samples (NiNPs: 99 mV dec^{-1} and graphene: 235 mV dec^{-1}). Although the Tafel slope of NiNPs-G is larger than that of Ni oxyhydroxide catalyst (60 mV dec^{-1}), this value is still much

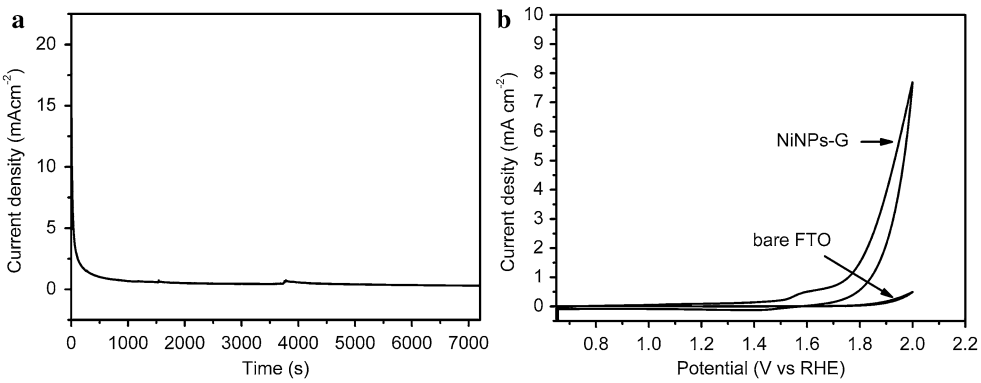

Fig. 4 **a** Controlled potential electrolysis of NiNPs-G at 1.56 V versus RHE. **b** CVs of NiNPs-G and bare FTO electrodes in 2 M phosphate buffer solution

smaller that those of N-doped graphene film-confined nickel nanoparticles (188.6 mV dec^{-1}) [14] and Ni_3S_2 nanorods/Ni foam composite (159.3 mV dec^{-1}) [24]. Further experiments with NiNPs-G showed a very similar catalytic current with the scan rates increasing from 5 to 100 mV s^{-1}, corresponding to the highly efficient transport and favorable catalytic kinetics within electrodes (Fig. 3c). Figure 3d shows the electrochemical impedance spectroscopy (EIS) data of NiNPs-G and NiNPs. From the plots, we can learn that the NiNPs-G displays bulk resistance, and charge-transfer resistance than NiNPs, indicating that the NiNPs-G exhibits higher conductivity because of the presence of graphene. Thus, compared to NiNPs, NiNPs-G thus exhibits more favorable OER kinetics.

In addition to the highly catalytic activity, good corrosion durability is vital for an advanced electrocatalyst for OER. We examined the durability of these catalyst using cyclic voltammograms (CVs) measurements for scanning 1,000 cycles from 0.964 to 1.964 V versus RHE with a scan rate of 100 mV s^{-1} in 0.1 M KOH. Figure 3e shows that NiNPs-G has good stability in alkaline electrolyte with less than 17 % anodic current loss during 1,000 cycles. Figure 3f shows the current–time chronoamperometric responses to OER on NiNPs-G and NiNPs catalysts at an overpotential of 384 mV. Although current densities of both two catalysts decrease with time, NiNPs-G exhibits a relatively slow decay rate, maintaining 86 % of their initial currents even after 45,000 s, whereas the OER current response for NiNPs decreases nearly 40 %. We attempted to quantify the active sites according to reported method [11]. The turnover frequency (TOF) was calculated from the steady-state current obtained from controlled potential electrolysis. The current gives a value of electrons passed per second. Because water oxidation is a four electron process this value is divided by four to give the number of oxygen molecules formed per second. The number of Ni atoms can be calculated by integration of the CVs (Fig. 4), 5.71×10^{-5} C or 5.92×10^{-10} mol Ni. The TOF of NiNPs-G was calculated to be 2.4 s^{-1} at overpotential of 330 mV, which is higher than those of hydrous nickel oxide electrodes (1.2 s^{-1}) [25] and gold-supported nickel oxide catalysts (1.9 s^{-1}) [26]. All of these results indicate that NiNPs-G shows superior durability over NiNPs catalyst due to the presence of graphene facilitating the electrons transport in the hybrid film.

4 Conclusions

Simultaneous electrochemical reduction of GO and Ni^{2+} has proved to be an effective strategy toward one-step preparation of NiNPs-G. As OER electrocatalyst, such NiNPs-G exhibits high efficiency with an onset potential of 1.564 V ($\eta = 334$ mV) and a tafel slope of 81 mV dec^{-1}, as well as good stability. Our present study is important because it provides us a general methodology for facile, rapid, and direct deposition of metal nanostructures-graphene hybrid film on conductive substrates toward electrocatalysis and other applications.

References

1. Walter MG, Warren EL, McKone JR, Boettcher SW, Mi Q, Santori EA, Lewis NS (2010) Solar water splitting cells. Chem Rev 110:6446–6473
2. Zhong DK, Gamelin DR (2010) Photoelectrochemical water oxidation by cobalt catalyst ("Co-Pi")/alpha-Fe_2O_3 composite photoanodes: oxygen evolution and resolution of a kinetic bottleneck. J Am Chem Soc 132:4202–4207
3. Hurst JK (2010) In pursuit of water oxidation catalysts for solar fuel production. Science 328:315–316
4. Liu X, Wang F (2012) Transition metal complexes that catalyze oxygen formation from water: 1979–2010. Coord Chem Rev 256:1115–1136
5. Gust D, Moore TA, Moore AL (2009) Solar fuels via artificial photosynthesis. Acc Chem Res 42:1890–1898
6. Fang Y, Liu Z (2010) Mechanism and Tafel lines of electro-oxidation of water to oxygen on RuO_2 (110). J Am Chem Soc 132:18214–18222
7. Kanan MW, Nocera DG (2008) In situ formation of an oxygen-evolving catalyst in neutral water containing phosphate and Co^{2+}. Science 321:1072–1075
8. Najafpour MM, Ehrenberg T, Wiechen M, Kurz P (2010) Calcium manganese (III) oxides ($CaMn_2O_4{\cdot}xH_2O$) as biomimetic oxygen-evolving catalysts. Angew Chem Int Ed 49:2233–2237

9. Suntivich J, May KJ, Gasteiger HA, Goodenough JB, Shao-Horn Y (2011) A Perovskite oxide optimized for oxygen evolution catalysis from molecular orbital principles. Science 334:1383–1385
10. Liang Y, Li Y, Wang H, Zhou J, Wang J, Regier T, Dai H (2011) Co_3O_4 nanocrystals on graphene as a synergistic catalyst for oxygen reduction reaction. Nat Mater 10:780–786
11. Kent CA, Concepcion JJ, Dares CJ, Torelli DA, Rieth AJ, Miller AS, Hoertz PG, Meyer TJ (2013) Water oxidation and oxygen monitoring by cobalt-modified fluorine-doped tin oxide electrodes. J Am Chem Soc 135:8432–8435
12. Subbaraman R, Tripkovic D, Chang KC, Strmcnik D, Paulikas AP, Hirunsit P, Chan M, Greeley J, Stamenkovic V, Markovic NM (2012) Trends in activity for the water electrolyser reactions on 3d M(Ni Co, Fe, Mn) hydr(oxy)oxide catalysts. Nat Mater 11:550–557
13. Singh A, Chang SLY, Hocking RK, Bach U, Spiccia L (2013) Highly active nickel oxide water oxidation catalysts deposited from molecular complexes. Energy Environ Sci 6:579–586
14. Chen S, Duan J, Ran J, Jaroniec M, Qiao S (2013) N-doped graphene film-confined nickel nanoparticles as a highly efficient three-dimensional oxygen evolution electrocatalyst. Energy Environ Sci 6:3693–3699
15. Hummers WS, Offeman RE (1958) Preparation of graphitic oxide. J Am Chem Soc 80:1339
16. Gao J, Liu F, Ma N, Wang Z, Zhang X (2010) Environment-friendly method to produce graphene that employs vitamin C and amino acid. Chem Mater 22:2213–2218
17. Li Z, Yao Y, Lin Z, Moon K-S, Lin W, Wong C (2010) Ultrafast, dry microwave synthesis of graphene sheets. J Mater Chem 20:4781–4783
18. Ramesha GK, Sampath S (2009) Electrochemical reduction of oriented graphene oxide films: an in situ Raman spectro electrochemical study. J Phys Chem C 113:7985–7989
19. Chen L, Tang Y, Wang K, Liu C, Luo S (2011) Direct electrodeposition of reduced graphene oxide on glassy carbon electrode and its electrochemical application. Electrochem Commun 35:133–137
20. Ye W, Zhang X, Chen Y, Du Y, Zhou F, Wang C (2013) Pulsed electrodeposition of reduced graphene oxide on glass garbon electrode as an effective support of electrodeposited Pt microspherical particles: nucleation studies and the application for methanol electro-oxidation. Int J Electrochem Sci 8:2122–2139
21. Chen S, Qiao S (2013) Hierarchically porous nitrogen-doped graphene $NiCo_2O_4$ hybrid paper as an advanced electrocatalytic water-splitting material. ACS Nano 7:10190–10196
22. Wang J, Zhong H, Qin Y, Zhang X (2013) An efficient three-dimensional oxygen evolution electrode. Angew Chem Int Ed 52:5248–5253
23. Trasatti S (ed) (1981) Electrodes of conductive metallic oxides. Elsevier, New York
24. Zhou W, Wu X, Cao X, Huang X, Tan C, Liu H, Wang J, Zhang H (2013) Ni_3S_2 nanorods/Ni foam composite electrode with low overpotential for electrocatalytic oxygen evolution. Energy Environ Sci 6:2921–2924
25. Godwin I, Lyons M (2013) Enhanced oxygen evolution at hydrous nickel oxide electrodes via electrochemical ageing in alkaline solution. Electrochem Commun 32:39–42
26. Yeo B, Bell A (2012) In situ Raman study of nickel oxide and gold-supported nickel oxide catalysts for the electrochemical evolution of oxygen. J Phys Chem C 116:8394–8400